Magnetic properties of AlPdMn approximant phases

1999 J. Phys.: Condens. Matter 11 10419

(http://iopscience.iop.org/0953-8984/11/50/331)

J. Phys.: Condens. Matter **11** (1999) 10419–10435. Printed in the UK PII: S0953-8984(99)07836-4

Magnetic properties of AlPdMn approximant phases

F Hippert†, V Simonet†[+], G Trambly de Laissardière‡§, M Audier‖ and Y Calvayrac¶

† Laboratoire de Physique des Solides (UMR CNRS/UPS), Bâtiment 510, Université de Paris-Sud, F-91405 Orsay Cédex, France
‡ LPTM, Université de Cergy-Pontoise, BP 222, 95302 Cergy-Pontoise Cédex, France
§ Laboratoire Léon Brillouin (CEA-CNRS), CE Saclay, 91191 Gif sur Yvette Cédex, France
‖ LMGP (UMR CNRS 5628), ENSPG, BP46, 38402 Saint Martin d'Hères, France
¶ CECM/CNRS, 15 rue G Urbain, F-94407 Vitry Cédex, France

Received 15 September 1999

Abstract. We investigated the magnetic properties of the following approximants of quasicrystals in the Al(Si)–Pd–Mn system: two cubic compounds, 1/1-$Al_{68}Pd_{11}Mn_{14}Si_7$ and 2/1-$Al_{70}Pd_{24}Mn_6$, and three orthorhombic compounds ξ'-$Al_{71.9}Pd_{23.5}Mn_{4.6}$, T-$Al_{73.1}Pd_{5.2}Mn_{21.7}$, and T-$Al_{78.5}Pd_{4.9}Mn_{16.6}$. No magnetic Mn atoms are present in the 2/1 and ξ' phases or in the Mn-poor T phase. In contrast, a fraction of the Mn atoms carry magnetic moments in the Mn-rich T phase in which a spin-glass transition occurs at 14 K, and in the 1/1 phase in which a ferromagnetic transition occurs at 8.8 K. The crystallographic sites responsible for the magnetism were identified from spin-polarized band-structure calculations; this allows us to discuss the origin of magnetism in both approximant and quasicrystal structures.

1. Introduction

While most stable quasicrystalline (QC) alloys exhibit a temperature-independent negative magnetic susceptibility like, for instance, icosahedral AlCuFe and AlPdRe phases [1, 2], the stable icosahedral and decagonal AlPdMn phases exhibit Curie-like terms [3–6]. Their magnetic properties are similar to those of metastable Al(Si)Mn quasicrystals [7]. Spin-glass transitions occur at low temperature in these AlPdMn and Al(Si)Mn quasicrystals. Low values for the Curie constant suggest that only a few per cent of the Mn atoms carry a magnetic moment, the origin of which has been widely debated. The moment formation was shown to be affected by the presence of a pseudo-gap in the density of states at the Fermi level and by the hybridization between Al s–p and Mn d states [8–11]. The question was then raised of whether magnetic Mn atoms are an intrinsic property of the quasicrystalline phases or only associated with structural defects. In this latter case, a AlPdMn quasicrystal of perfect structure should be non-magnetic. However, spin-polarized band-structure calculations based on quasicrystalline AlPdMn models [10] show that the formation of magnetic moments on Mn atoms is extremely sensitive to their local environment and only occurs at a few special Mn sites. These results suggest therefore that magnetism is an intrinsic property of the AlPdMn QC phases. Nevertheless a detailed comparison of these band-structure calculations with measured magnetic properties is difficult because the present determination of the quasicrystal structure only involves about 85% of the atomic sites.

[+] Present address: Laboratoire de Cristallographie, CNRS, 25 Avenue des Martyrs, BP 166, 38042 Grenoble Cédex, France.

0953-8984/99/5010419+17$30.00

This difficulty does not occur in studies of approximants. Let us recall that approximants are periodic phases of large unit cells with structures closely related to those of quasicrystals [12]. Some approximants can be described as packings of large icosahedral clusters like, for instance, Mackay (54 atoms) or Bergman (104 atoms) clusters [13] which are also found in QC structural models. High-order approximants (with very large unit cells) exhibit the same electronic properties as QC phases, namely a reduced density of electronic states at the Fermi level and anomalous transport properties such as a very high electrical resistivity with a negative temperature coefficient [14]. Provided that the magnetic properties of approximants are similar to those of related QC phases, their study should then shed light on the origin of magnetism in QC phases. For example, in a recent work we were able to identify the crystallographic site occupied by magnetic Mn atoms in the hexagonal μ-Al_4Mn phase [15] and conclude that similar sites might also exist in related Al(Si)Mn QC phases. In the Al(Si)–Pd–Mn system, using the results of recent determinations of the structure of several approximant phases (cubic 1/1 and 2/1 phases [16, 17] and orthorhombic ξ' and T phases [18–20]) the same type of approach is now possible. The present work is therefore devoted to an experimental and theoretical study of the magnetic properties of these phases. By combining results of magnetization measurements and spin-polarized band-structure calculations, we can identify the magnetic sites.

The different sections of this paper are organized as follows. The structure of the approximant phases studied is recalled in section 2, laying emphasis on Mn environments. Results of magnetic measurements are presented in section 3 and spin-polarized band-structure calculations, using the LMTO method, are presented in section 4. The identification of the magnetic sites and the origin of the magnetism are discussed in section 5. Finally, the magnetic properties of these approximants are compared to those of quasicrystals in section 6.

2. Sample description

The ternary Al–Pd–Mn phase diagram has been investigated in detail by several teams [21–24] in the vicinity of icosahedral and decagonal quasicrystalline phases. Ternary orthorhombic phases, the so-called ξ, ξ', R and T phases (space group $Pnma$), have been reported in [22] and their conditions of stability have been clarified in [24]. Both the ξ and ξ' structures are approximants of the icosahedral quasicrystal as they are related to a 6D periodic description of the icosahedral structure through a 6D shear matrix [22,25]. From similar demonstrations, both the T and R structures have been shown to be approximants of the decagonal quasicrystal [25]. Note that the ξ and ξ' phases on one hand, and the R and T phases on the other hand, have the same unit-cell volume and are related in each case by a 3D shear transformation where the shear is characteristic of phason shifts [25]. The two cubic phases (2/1 and 1/1, space group $Pm3$ [16, 17]) can be obtained in the cut-and-project method by a simple rotation of the cut used to build the icosahedral structure so that its slope becomes a rational approximant (2/1 or 1/1) of the golden mean $\tau = (1 + \sqrt{5})/2$. The 1/1 phase is stabilized by the presence of 7% Si. The 2/1 phase studied in reference [17] contains 1.3% Si (not distinguished from Al in the structural analysis). However, this phase was discovered in the $Al_{70}Pd_{26}Mn_4$ alloy [26]. We have found that it is stable in this ternary system and that the $Al_{70}Pd_{24}Mn_6$ alloy is single phased.

In the present work, only samples of the 1/1, 2/1, ξ' and T phases were studied. (The amounts of the single-phased samples of the ξ and R phases were too small for us to perform magnetic measurements). Crystallographic data on these phases are gathered in table 1. For each Mn crystallographic site, the numbers of atoms in the unit cell, the coordinations and the ranges of first-neighbour distances are reported. The compositions given in table 1 are those deduced from the structure analysis. Note that the 1/1, 2/1 and ξ' approximants are only found

Table 1. The structure of AlPdMn approximants. For each phase, the space group, the reference to the crystallographic study, the lattice parameter(s), the composition deduced from the structural analysis and the number of atoms per unit cell are first given. Then, for each Mn Wyckoff site, the number of Mn per unit cell and the number, the nature and the distance range of the first neighbours are given. For the T phase, both the structure of the Mn-rich sample (24.4%) studied in reference [19] and the structure of the sample with the lowest Mn content (15.4%) are given. For the 2/1 and Mn-rich T phases, only an averaged environment can be defined because of the chemical disorder.

Space Group Reference	Lattice parameter (Å)	Composition Atoms/cell	Mn site	Mn/cell	Neighbours	Distance (Å)
1/1	$a = 12.281$	$Al_{66.3}Pd_{12}Mn_{14.7}Si_7$	Mn(4)	6	10Al	(2.447–2.592)
$Pm3$		122.7	Mn(5)	12	7Al–5Mn	(2.374–2.657)
[16]						
2/1	$a = 20.211$	$Al_{69.6}Pd_{24.3}Mn_{6.1}$	Mn(14)	6	10Al	(2.450–2.624)
$Pm3$		512.8	Mn(15)	10.3	7.03Al–1.23Mn 0.29Pd	(2.393–2.923)
[17]			Mn(17)	3.96	6.94Al–0.86Mn 2.63Pd	(2.478–3.089)
			Mn(18)	10.8	6.78Al–1.31Mn 2.63Pd	(2.492–3.042)
ξ'	$a = 23.541$	$Al_{71.47}Pd_{22.75}Mn_{5.78}$	Mn(8)	8	12Al	(2.657–2.814)
$Pnma$	$b = 16.566$	276.6	Mn(12)	8	11Al	(2.370–2.717)
[18]	$c = 12.339$					
T	$a = 14.717$	$Al_{72.4}Pd_{3.2}Mn_{24.4}$	Mn(1)	4	9Al	(2.409–2.577)
$Pnma$	$b = 12.510$	156	Mn(2)	4	10.4Al–1.6Mn	(2.483–2.792)
[19]	$c = 12.594$		Mn(3)	4	10.1Al–1.9Mn	(2.474–2.757)
			Mn(4)	4	9.7Al–2.3Mn	(2.471–2.782)
			Mn(5)	8	10.25Al–1.75Mn	(2.424–2.913)
			TM(1)	4	10.43Al–2.95Mn 0.62Pd	(2.579–3.167)
			TM(2)	4	10.28Al–3.1Mn 0.62Pd	(2.589–3.230)
			TM(3)	2.4	9.28Al–3.1Mn 0.62Pd	(2.592–3.077)
			TM(4)	2.4	8.93Al–3.45Mn 0.62Pd	(2.584–3.077)
			TM(5)	1.2	8.6Al–4.4Mn	(2.652–3.063)
T		$Al_{81.4}Pd_{3.2}Mn_{15.4}$	Mn(1)	4	9Al	(2.409–2.577)
			Mn(2)	4	12Al	(2.483–2.792)
			Mn(3)	4	11Al–1Mn	(2.474–2.757)
			Mn(4)	4	11Al–1Mn	(2.471–2.782)
			Mn(5)	8	12 Al	(2.424–2.913)

in narrow composition domains, while the T phase exists over a relatively wide composition range, corresponding mainly to a variation of the Al/Mn ratio.

In the cubic 1/1-$Al_{66.3}Pd_{12}Mn_{14.7}Si_7$ phase [16], there are two Wyckoff sites occupied by Mn atoms. The Mn(5) atoms form an icosahedron with a small edge (2.65 Å). This seems to be a specific feature of this phase, not observed in the other approximant structures. (For comparison, the edge of the Mn icosahedron within a Mackay cluster in the cubic α-$Al_{72.45}Mn_{17.4}Si_{10.15}$ phase is 5.1 Å [27].) Each Mn(5) atom is surrounded by five Mn and seven Al atoms forming a slightly distorted icosahedron. The Mn(4) atom lies between the

clusters located at the origin and the centre of the unit cube and is surrounded by ten Al atoms.

Very large icosahedral clusters have also been defined in the cubic 2/1-$Al_{69.6}Pd_{24.3}Mn_{6.1}$ phase [17]. There are five different Mn Wyckoff sites, labelled Mn(14) to Mn(18). However, as the partial occupation of site 16 by Mn atoms is less than 3%, this site is not considered in table 1. Mn(15) and Mn(17) + Mn(18) belong to the cluster at the origin of the unit cell and are located on two different shells of radius 7.3 and 8.2 Å respectively. Mn(14) lies between the clusters located at the origin and the centre of the unit cube. It is characterized by a smaller coordination polyhedron than those of the three other Mn sites. Note that none of these Mn sites has an icosahedral environment.

The orthorhombic ξ'-$Al_{71.47}Pd_{22.75}Mn_{5.78}$ phase [18] contains two Mn Wyckoff sites. Mn(8) is surrounded by twelve Al atoms located at the vertices of a slightly distorted icosahedron. Mn(12) is surrounded by an incomplete icosahedral shell of about eleven Al, itself surrounded by twelve Pd atoms also located at the vertices of a larger icosahedron.

The orthorhombic cell of the T-$Al_{72.4}Pd_{3.2}Mn_{24.4}$ phase contains 156 atomic sites distributed on 25 Wyckoff sites where five are occupied by Mn atoms only, five by Al/Mn mixtures with various Al/Mn ratios, one by a Pd/Al mixture and fourteen by Al atoms [19, 20]. The presence of sites occupied by Al/Mn mixtures (sites TM(1) to TM(5) in reference [19]) has to be related to the large composition domain of the T phase [24]. On one hand, the structural data of reference [19], summarized in table 1, correspond to a sample with a Mn content (24.4%) close to the maximum possible value. Due to the varying chemical environment of each Mn site, resulting from the partial occupations, only an averaged environment can be defined. On the other hand, the composition calculated assuming that the sites TM(1) to TM(5) are only occupied by Al atoms, $Al_{81.4}Pd_{3.2}Mn_{15.4}$, corresponds roughly to the other end of the existence domain of the T phase (with the lowest Mn content). For this peculiar composition, the first neighbours of the five Mn sites are entirely determined (table 1). (The remaining chemical disorder concerns only the partial occupancy of site TM(6) by Al and Pd atoms and does not affect the first neighbours of Mn atoms.) The structure of the T phase with the minimum Mn content (15.4%) can be conveniently described by identifying icosahedral clusters centred on the Mn sites, following an approach proposed for several intermetallic Al–Mn or Al–Cr structures [28]. Indeed all Mn atoms, except Mn(1), are coordinated by icosahedra, i.e. each of these Mn atoms is surrounded by twelve atoms located at the vertices of a slightly distorted icosahedron. On account of the *Pnma* space group, the T phase structure appears to be a stacking of two types of icosahedral cluster layer perpendicular to the ***b***-axis and centred at $y = 1/2$ and $y = 1/4$ (the mirror plane) (figure 1). In the corrugated layer at $y = 1/2$, the icosahedral clusters, centred on Mn(5), are separated and have a fivefold axis parallel to the ***b***-axis. In the flat layer, at $y = 1/4$, the clusters, centred on Mn(2), Mn(3) and Mn(4), exhibit a twofold axis parallel to the ***b***-axis. They are either linked to each other by vertices or triangular faces or overlap along a pseudo-fivefold axis, such that the Mn atom at the centre of one icosahedron serves as a vertex for a neighbouring icosahedron and vice versa. (Mn(3) and Mn(4) are thus first neighbours.) The Mn (1) site of lower coordination (nine Al) is also in the layer at $y = 1/4$. The Pd site and one Al site are located between icosahedral clusters of the $y = 1/2$ layer. Between the two layers, the clusters are linked by triangular faces. In addition, it should be noted that the ternary T phase is not isomorphic with the binary T-Al_3Mn phase [29], although the structures of these two phases are closely related. The reason is twofold:

(i) Pd atoms do not randomly substitute for Al or Mn atoms but occupy a particular Wyckoff site in the ternary phase and

(ii) several Mn sites are different in these two structures.

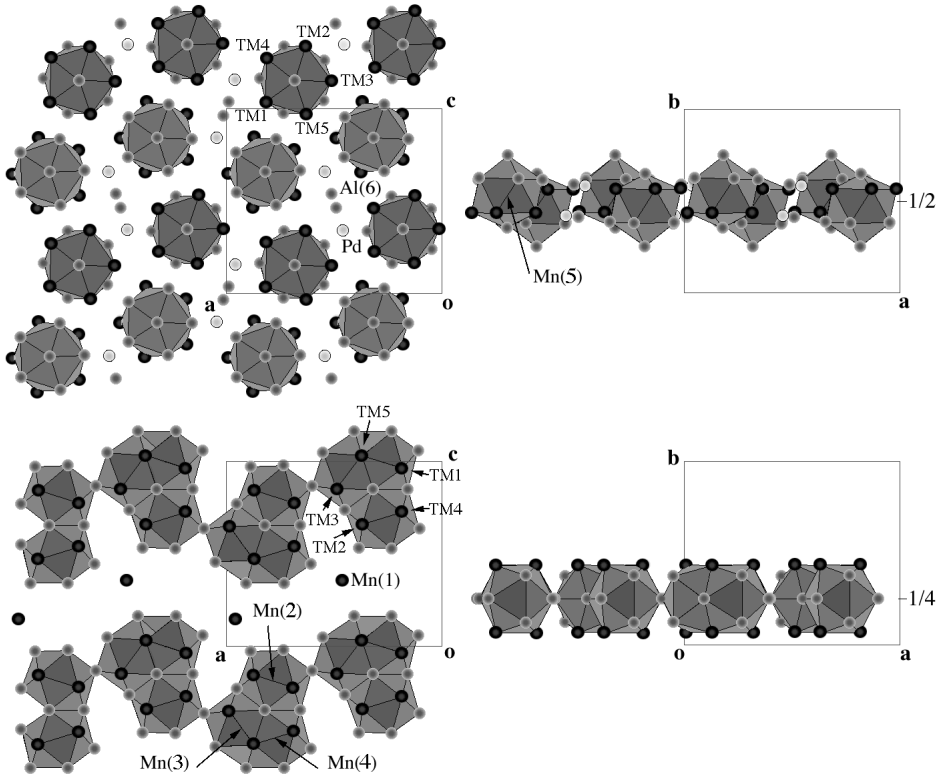

Figure 1. Interpretation of the crystal structure of the T-$Al_{81.4}Pd_{3.2}Mn_{15.4}$ phase in terms of icosahedral clusters centred on the Mn sites, denoted as Mn(1) to Mn(5), according to the crystallographic data of reference [19]. Al atoms are represented as lightly shaded balls. The Al sites occupied by Al/Mn mixtures in T phases with higher Mn content (denoted as TM(1) to TM(5) in the figure) are represented as dark balls. Taking into account the *Pnma* space group, two types of layer perpendicular to the ***b***-axis are considered: a corrugated layer at $y = 1/2$ and a flat one at $y = 1/4$ (the mirror plane).

The samples studied are presented in table 2. The 1/1 and 2/1 cubic phase samples are ribbons produced by planar flow casting. They were annealed respectively at 600 °C for 62 h and 815°C for 2 h. Their nominal compositions (i.e. those of the liquid alloys) are indicated in table 2. The 1/1 cubic sample (a) contains 7% Si. Its composition is very close to that given in reference [16]. However, this sample is not single phased: some weak x-ray lines present in the diffraction diagram could not be indexed. The 2/1 cubic sample (b) is single phased (within the accuracy of x-ray diffraction). Its composition, $Al_{70}Pd_{24}Mn_6$, is close to the one deduced from the crystallographic study of reference [17] where no distinction was made between Al and Si atoms. The ξ' sample (c) was obtained as a single crystal by Czochralski growth. Because of non-congruent fusion of this phase, its composition differs from that of the melt. Both the nominal composition of the initial liquid alloy and the composition of the single crystal analysed by x-ray wavelength-dispersive spectroscopy (XWDS) are given in table 2. The T phase samples (d) and (e) were obtained by Bridgman growth from two different liquid-alloy compositions. These samples are polycrystalline with very large grain sizes of several millimetres. Small amounts of foreign phases precipitated at the grain boundaries (icosahedral, ξ' and Al/ξ' eutectic in sample (d), ξ' and Al/ξ' eutectic in sample (e)) have been observed in

Table 2. Samples studied: structure, composition and magnetic properties. For ribbons, nominal compositions are given. For ingots, both the nominal composition of the initial liquid alloy (within parentheses) and the composition analysed by XWDS are given. In the last three columns we report the temperature range and the parameters of the fit of the susceptibility by a Curie law: $\chi(T) = \chi_0 + C/T$. In the 2/1 phase, a T^2-contribution must be added. In the 1/1 phase, because of ferromagnetic interactions, the susceptibility is described by $\chi(T) = \chi_0 + C/(T - \Theta)$ with $\Theta = 20$ K.

State	Sample	Composition	T-range (K)	C (emu K g^{-1})	$10^6\chi_0$ (emu g^{-1})
Ribbons	a, 1/1	$Al_{68}Pd_{11}Mn_{14}Si_7$	30–300	1.03×10^{-3}	0
Ribbons	b, 2/1	$Al_{70}Pd_{24}Mn_6$	5–300	1.7×10^{-6}	−0.407
Single crystal	c, ξ'	$Al_{71.9}Pd_{23.5}Mn_{4.6}$ ($Al_{77.5}Pd_{19}Mn_{3.5}$)	5–300	0.7×10^{-6}	−0.136
Ingot	d, T	$Al_{73.1}Pd_{5.2}Mn_{21.7}$ ($Al_{73.8}Pd_{7.2}Mn_{19}$)	30–100 150–300	1.66×10^{-3} 2.15×10^{-3}	5.0 0.8
Ingot	e, T	$Al_{78.5}Pd_{4.9}Mn_{16.6}$ ($Al_{83.9}Pd_{8.1}Mn_8$)	150–300	5.0×10^{-5}	0.4

these samples. We have found that the compositions vary over a few at.% within each T phase sample: for the sample (d) Al: from 71.6 to 74.7; Pd: 3.7 to 7.0; Mn: 18.1 to 24.6; and for the sample (e) Al: from 78.2 to 78.7; Pd: 4.5 to 5.6; Mn: 15.7 to 17.2. Only average values are indicated in table 2. Note that the average Mn contents (respectively 21.7 and 16.6 Mn at.% for samples (d) and (e)) are close to the upper and lower limits of the composition domain of the T phase [24].

3. Magnetic properties

Using a superconducting quantum interference device magnetometer, we have measured the magnetization in the temperature range [5–300 K] and in magnetic fields up to 50 kOe. Complementary ac susceptibility measurements were performed as well on the 1/1 cubic phase in the temperature range [5–15 K] (using an ac field of 1 Oe at 13 Hz).

3.1. ξ' and 2/1 phases

The dc susceptibility of the 2/1 and ξ' phases is found to be nearly temperature independent (figure 2). Only very small Curie-like terms are detected. The measured Curie constants ($C = c^\star g^2 \mu_B^2 N_a S(S+1)/(3k_B M_a)$, where $c^\star$ is the atomic concentration of localized moments, S their spin and M_a the atomic mass) are reported in table 2. Assuming a spin value $S = 5/2$ and $g = 2$, they correspond to a concentration $c^\star$ of localized moments equal to 1.8×10^{-5} in the 2/1 phase (i.e. $c^\star/c = 3 \times 10^{-4}$, where c is the total Mn atomic concentration) and 7.5×10^{-6} in the ξ' phase (i.e. $c^\star/c = 1.6 \times 10^{-4}$). It is then difficult to decide whether this behaviour is intrinsic or due to very small quantities of foreign phases (unidentified by x-ray diffraction). We shall consider these samples as non-magnetic in the following.

At 300 K, the susceptibility of the 2/1 cubic phase ($\chi = -0.38 \times 10^{-6}$ emu g^{-1}) is negative and close to the value measured in AlCuFe and AlPdRe QC phases [1,2] and in an icosahedral $Al_{70.5}Pd_{22}Mn_{7.5}$ phase where the Curie contribution is nearly negligible [3]. The negative value

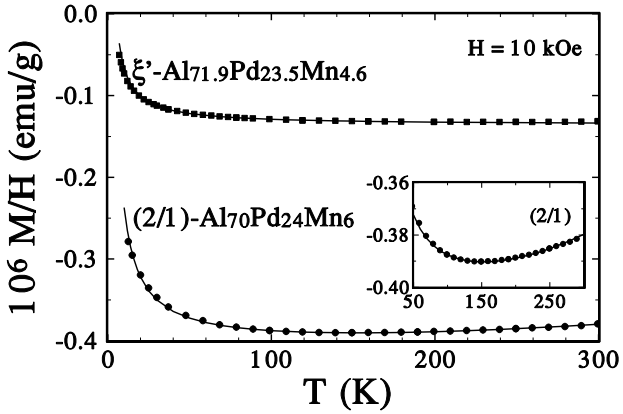

Figure 2. The temperature dependence of the dc magnetic susceptibility M/H ($H = 10$ kOe) for the 2/1 and ξ' phases. Inset: the 2/1 phase above 50 K. The solid lines are fits to $\chi(T) = \chi_0 + AT^2 + C/T$: see the text ($A = 0$ for the ξ' phase).

of the susceptibility is partly due to the low density of states (DOS) at the Fermi level resulting in a weak Pauli susceptibility of the conduction electrons. Additionally, the possibility of a strong Landau diamagnetism of conduction electrons has been proposed [30]. Unfortunately the large uncertainty of the Larmor contribution makes the determination of the electron contribution and any further analysis difficult. Above 150 K, an increase of the susceptibility with temperature occurs (see the inset of figure 2). The temperature dependence of the susceptibility can be fitted by $\chi(T) = \chi_0 + AT^2 + C/T$, where χ_0 accounts for the temperature-independent contribution. Such a T^2-term in χ, previously observed in AlCuFe and AlPdMn QC [1,4], has been ascribed to the presence of a sharp feature in the DOS near the Fermi level. Note that the T^2-coefficient measured in the 2/1 phase, $A = (0.24 \pm 0.03) \times 10^{-12}$ emu g^{-1} K^{-2}, is close to those measured for AlCuFe QC (0.43×10^{-12} [1]) and for AlPdMn QC (0.19 to 0.47×10^{-12} [4]).

In summary, the susceptibility of the 2/1 cubic approximant phase is very close to that of non-magnetic quasicrystalline phases, which indicates a similar DOS near E_F. In contrast, the magnetic behaviour of the ξ' phase is that of a usual metal. Its susceptibility is larger ($\chi = -0.134 \times 10^{-6}$ emu g^{-1} at 300 K) and can be fitted by $\chi(T) = \chi_0 + C/T$ (table 2). If a T^2-contribution is introduced, the A-value is less than 0.02×10^{-12} emu g^{-1} K^{-2}, supporting the conclusion that this term is not present in the susceptibility of this phase.

3.2. T phases

Large Curie-like terms are detected in the T phase sample (d) with 21.7% Mn (figure 3). However, a strict Curie behaviour is not obeyed: the data can be fitted by a Curie law $\chi(T) = \chi_0 + C/T$ only in a restricted temperature range and both C and χ_0 depend slightly on the temperature range analysed (table 2). In contrast with the case of the 2/1 and ξ' phases, the χ_0-value is found to be positive, which might be ascribed to a larger Pauli contribution in this T phase sample. The Curie-like behaviour is without any doubt an intrinsic property of the T phase, as neither the foreign phases (icosahedral and ξ') nor the Al/ξ' eutectic, present in small quantities in the sample, can be responsible for the large Curie constant measured. The C-value is about ten times larger than those measured for icosahedral AlPdMn single crystals [4]. The ξ' phase is non-magnetic (section 3.1). The eutectic is also non-magnetic: no Curie term was detected for ingots containing an appreciable amount of eutectic [31]. From the

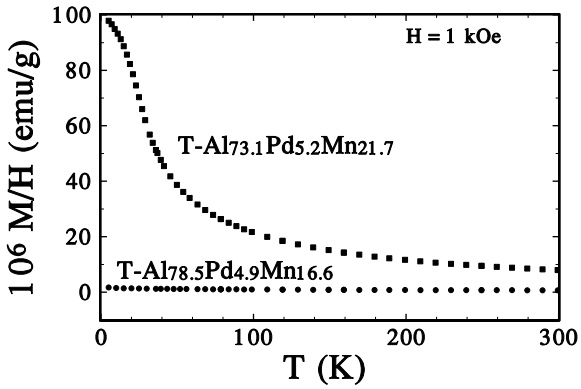

Figure 3. The temperature dependence of the dc magnetic susceptibility M/H ($H = 1$ kOe) in the T phase samples with 21.7% and 16.6% Mn.

Curie constants given in table 2 and assuming that all of the Mn atoms (atomic concentration $c = 0.217$) carry the same spin, one deduces that $S = 0.4$ and 0.49 in the temperature ranges [30 K–100 K] and [150 K–300 K] respectively, with $g = 2$. By analogy with QC phases, we might also consider that only a fraction of the Mn atoms carry magnetic moments. In this case, assuming that the spin is equal to its maximum value $S = 5/2$, one gets a minimum value for the atomic concentration in magnetic Mn: $c^\star = 1.4 \times 10^{-2}$ (i.e. $c^\star/c = 0.065$) and $c^\star = 1.83 \times 10^{-2}$ (i.e. $c^\star/c = 0.084$) in the two temperature ranges.

At lower temperature, below 16 K, strong deviations from a Curie behaviour occur revealing magnetic interactions. The magnetization measured in a given field after field cooling in that field (the FC process) is nearly temperature independent. In contrast, the magnetization measured in the same field, but after cooling in zero field (the ZFC process), increases with increasing temperature and shows a maximum around 14 K (figure 4(a)). Above 16 K both sets of data coincide and the magnetization does not depend on the cooling process. Such a behaviour is reminiscent of spin glasses [32]. The maximum of the ZFC magnetization is slightly rounded, which reveals a small distribution of spin-glass temperature T_g, certainly linked to the Mn concentration variations detected in that sample (see section 2). In addition, remanent effects are observed. In figure 4(b) the remanent magnetization M_r measured at 5 K in zero field is plotted as a function of the cooling field H_c for two different procedures. The thermoremanent magnetization (TRM) is measured in zero field after cooling from above T_g down to 5 K in the field H_c. The isothermal remanent magnetization (IRM) is measured after zero-field cooling and then applying and switching off H_c at 5 K. The field dependence of M_r is that of a typical spin glass. The usual time dependence of M_r is also observed: for example after field cooling under 10 kOe down to 5 K and switching off the field, M_r decreases by 13% in ten minutes. All these observations are therefore strong indications in favour of a spin-glass transition at $T_g \sim 14$ K in the T-$Al_{73.1}Pd_{5.2}Mn_{21.7}$ phase†. One must emphasize that a spin-glass behaviour requires the frustration of magnetic interactions which can only be achieved by there being some disorder in the positions of magnetic Mn. This point will be discussed in section 5.

The other T phase sample (e), with 16.6% Mn, exhibits a much smaller magnetism (figure 3). The data cannot be described by a Curie law: a plot of χ versus $1/T$ reveals

† Strictly speaking, the divergence of the non-linear susceptibility should be established in order to definitively ascertain the existence of a spin-glass transition. This is beyond the scope of the present paper.

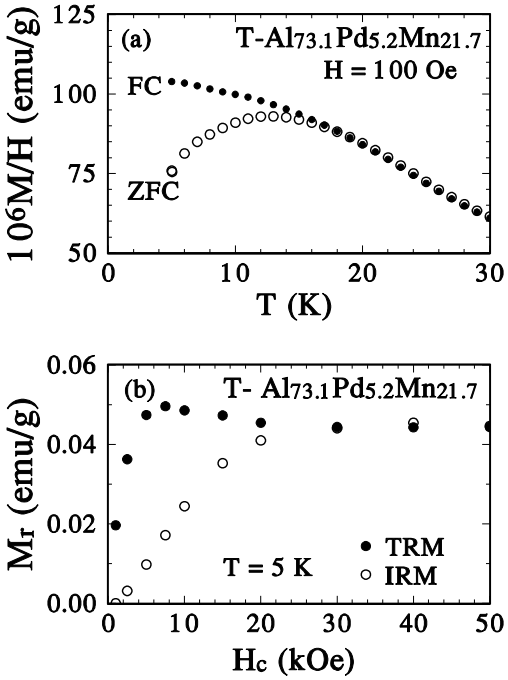

Figure 4. The T-$Al_{73.1}Pd_{5.2}Mn_{21.7}$ phase. (a) Comparison of the field-cooled (FC) and zero-field-cooled (ZFC) magnetization measured in 100 Oe. (b) Remanent magnetization measured at 5 K in zero field, ten minutes after switching off the magnetic field H_c, either after field cooling from 20 K (thermoremanent magnetization, TRM) or after zero-field cooling and applying H_c at 5 K (isothermal remanent magnetization, IRM).

a strong continuous curvature. Further investigations would be needed in order to understand this behaviour and check its intrinsic character. Nevertheless a Curie fit can be performed over the restricted temperature range [150 K–300 K]. As the C-value obtained (table 2) is about 40 times smaller than the one measured for sample (d), the T-$Al_{78.5}Pd_{4.9}Mn_{16.6}$ phase will be considered as non-magnetic in the framework of the present study.

3.3. The 1/1 phase

The dc susceptibility of the 1/1 sample, measured in 1 kOe (figure 5), strongly increases with decreasing temperature below 30 K which suggests the existence of a ferromagnetic transition. This is confirmed by ac susceptibility measurements in the range [5 K–15 K] (see the inset of figure 5) which exhibit a maximum at $T_c = 8.8$ K. The ratio $\chi_{ac}(T = 8.8\,\mathrm{K})/\chi_{ac}(T = 15\,\mathrm{K})$ is equal to 60 and the maximum value of the ac susceptibility (0.36 emu cm^{-3}, using the density $d = 4.47$ g cm^{-3}) is larger than the demagnetization factor for a spherical sample ($3/4\pi$). Note that the demagnetization factor of the measured sample (i.e. small flakes in a cylindrical sample holder) cannot be accurately determined. This very large susceptibility value suggests that the observed ferromagnetism is indeed an intrinsic property of the 1/1 cubic phase and is not associated with secondary phases. In the range [30 K–300 K], the dc susceptibility data can be fitted by $\chi(T) = \chi_0 + C/(T - \Theta)$ with $\Theta = 20$ K (figure 5 and table 2). Assuming that all the Mn atoms carry the same spin, one deduces $S = 0.41$ from the measured Curie constant.

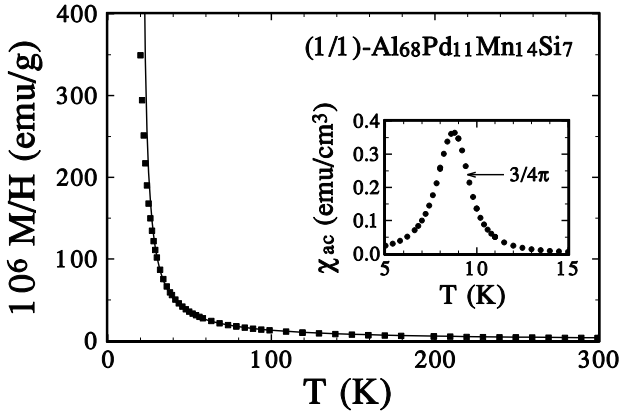

Figure 5. The temperature dependence of the dc magnetic susceptibility M/H ($H = 1$ kOe) in the 1/1 cubic phase. The solid line is a fit to $\chi(T) = \chi_0 + C/(T - \Theta)$: see the text. Inset: ac susceptibility data measured in a field of 1 Oe at 13 Hz in the range 5–15 K. The maximum value of the ac susceptibility is larger than the demagnetization factor for a spherical sample ($3/4\pi$).

4. LMTO calculations

Electronic and magnetic structures were calculated by the self-consistent *ab initio* method using a linear muffin-tin orbital technique (LMTO-ASA) [33]. The density functional formalism was used within the local spin-density approximation (LSDA) [34]. In the framework of the atomic sphere approximation (ASA), the sphere radii were chosen to obtain a good compromise between the sphere overlaps and the charge transfers between spheres, which resulted in less than 0.3 electron per atomic sphere. Combined corrections were used to correct errors from the overlapping of the spheres and the interstitial region. Electronic eigenstates were calculated from the diagonalization of the LMTO Hamiltonian. Because of computational time limitations, we could not carry out calculations for an approximant with too large a number of atoms in the unit cell. Therefore we studied by the LMTO method only the 1/1 and T phases. Their atomic distribution is homogeneous and their structures are rather compact so no empty spheres were necessary to fill up the space within the ASA. Orbitals up to angular momentum $l = 2$ were used to build the LMTO wave functions and the valence states were Al 3s, 3p, 3d, Si 3s, 3p, 3d, Mn 4s, 4p, 3d and Pd 5s, 5p, 4d. During the self-consistent procedure, the number of $\boldsymbol{k}$-points in the first Brillouin zone was 729 and 64 for 1/1 phase and T phase, respectively. It has been increased up to 512 for the final computation of the density of states of the T phase. For each phase, we performed first a LMTO calculation for a non-magnetic state, where all local moments were fixed to zero, and then a spin-polarized calculation. In this latter case, the initial value of gS was taken equal to 4 for Mn atoms (and for Pd atoms).

4.1. The 1/1 phase

We introduced two minor modifications in the structure of the cubic 1/1 phase determined by Sugiyama *et al* [16]. The mixed site Pd/Al(1) (Wyckoff position 1b) is occupied only by Pd atoms with an occupation factor equal to 1. The Si(14) atoms at Wyckoff position 6g ($x = 1/2$, $y = 0$, $z = 0.0516$) with an occupation factor equal to 0.45 are put at a Wyckoff site 3d ($x = 1/2$, $y = 0$, $z = 0$) with an occupation factor equal to 1. These modifications are necessary because the occupation factors have to be equal to 1 in LMTO calculations. The

composition of the model is therefore $Al_{65.9}Pd_{12.2}Mn_{14.6}Si_{7.3}$ and it contains 123 atoms per cubic cell (to be compared to 122.7 in the structure of reference [16]). The lattice parameter a was taken equal to 12.281 Å [16]. Note that this structural model differs from the one used by Hafner and Krajči for magnetic and electronic structure calculations in reference [9]. Starting from a description of the atomic structure of the QC phase in 6D and using a rational projection, these authors constructed an hypothetical 1/1 structure [35]. However, the local order of their model, as well as the number of non-equivalent sites, differ markedly from the results of the later crystallographic study [16].

The total DOS together with the local DOS at Mn(4) and Mn(5) sites, calculated without spin polarization, are shown in figure 6. They exhibit a spiky structure, like those observed previously in other approximant phases studied [35, 36]. The maximum in the total DOS around -4.2 eV is due to the Pd d states. The local DOS at the Al exhibits a narrow minimum near the Fermi level but this feature is nearly masked in the total DOS because of the strong Mn contribution. However, the Mn DOS differ markedly on the two Mn sites. At Mn(4) sites, the Mn d band is split into two parts (bonding and antibonding states). This splitting results from the sp–d hybridization and the diffraction by Bragg planes [8] (see section 5). The local DOS at Mn(4) exhibits therefore a pseudo-gap near the Fermi level. In contrast, no pseudo-gap is observed in the local DOS at Mn(5). The peculiar character of the local DOS at this latter site is probably influenced by the presence of five Mn(5) first neighbours leading to important d–d couplings. The spin-polarized LMTO calculation converges to a non-magnetic state ($S = 0$) at Mn(4) atoms (and at the Pd atom). In contrast, there is a localized magnetic moment on

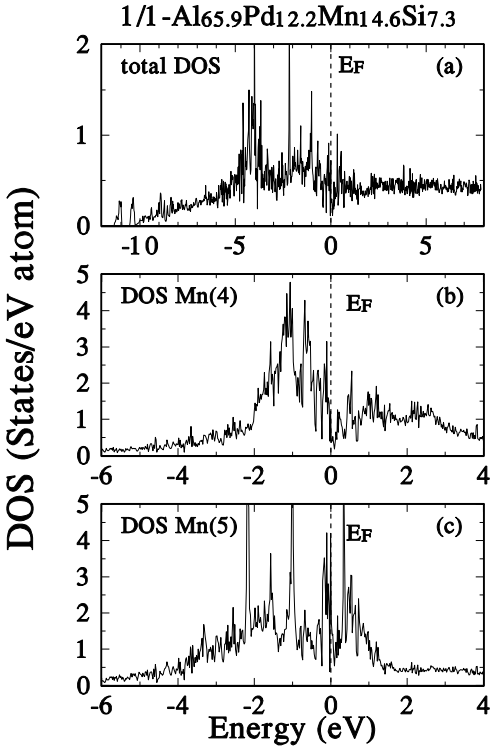

Figure 6. (a) The electronic structure of the 1/1-$Al_{65.9}Pd_{12.2}Mn_{14.6}Si_{7.3}$ phase, calculated without spin polarization: (a) the total DOS, (b) the partial DOS at Mn(4), (c) the partial DOS at Mn(5).

Mn(5) atoms, with a small gS-value of the order of 0.7. It should be emphasized that, in this calculation, all Mn(5) atoms are assumed to be equivalent and that therefore their magnetic moments are necessarily collinear.

4.2. The T phase

Starting from the structure of the T phase [19], we assumed that TM(1) to TM(5) are only occupied by Al atoms and that TM(6) is only occupied by Pd atoms. There are 156 atoms in the orthorhombic unit cell and the composition is $Al_{79.5}Pd_{5.1}Mn_{15.4}$. The lattice parameters were assumed to be identical to those of the Mn-rich T phase (table 1).

The total DOS, calculated without spin polarization, exhibits a broad minimum near the Fermi level (figure 7). The width of this pseudo-gap, of the order of 0.7 eV, is comparable to the values found in the literature for other approximants [9, 35, 36]. The maximum around -4.6 eV is due to the Pd d states. The average Mn d band has its maximum about -1.8 eV below the Fermi energy. Although the Fermi level is located in the minimum of the pseudo-gap, the local DOS at E_F is relatively high ($\sim$0.37 states eV^{-1}/atom). The same trend was previously observed in several approximants of decagonal phases [37] where, unlike in the AlPdMn icosahedral alloys [35], the Mn d band overlaps with the Fermi level and reduces the influence of the deep minimum observed in the Al sp band. However, this argument is only valid for the averaged d band: marked differences are observed between the local DOS

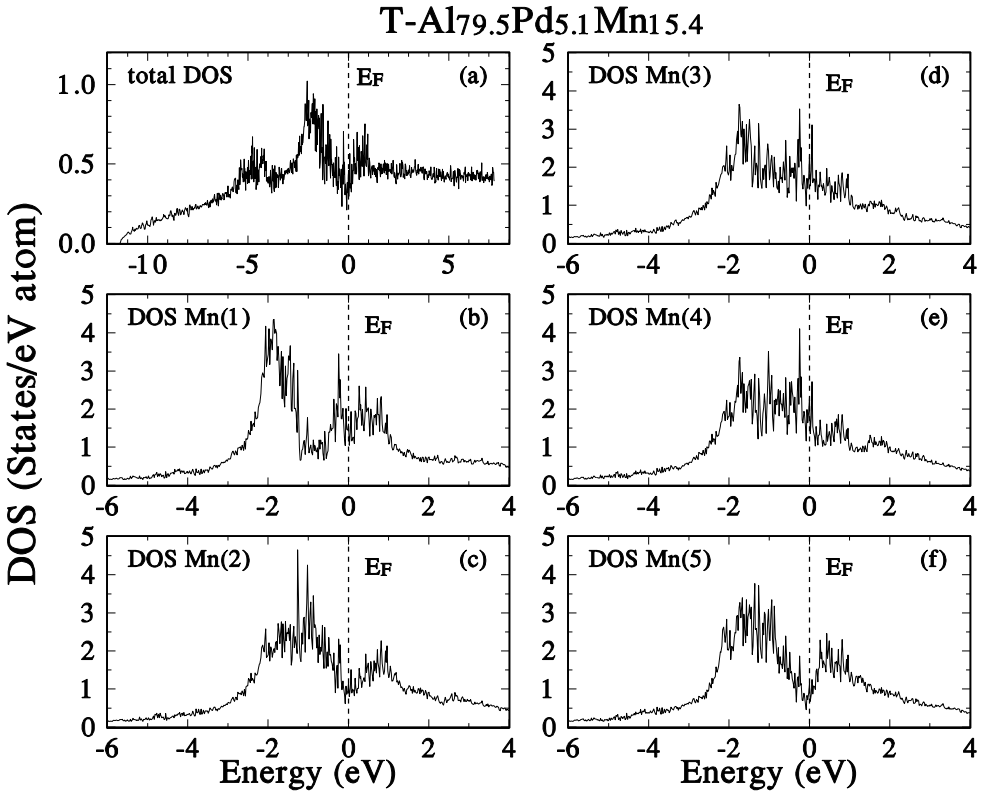

Figure 7. The electronic structure of the T-$Al_{79.5}Pd_{5.1}Mn_{15.4}$ phase: (a) the total DOS, (b) to (f) the partial DOS at Mn(1) to Mn(5).

at the five non-equivalent Mn sites, calculated without spin polarization (figure 7). The local DOS at Mn(2) and Mn(5), both surrounded by twelve Al in an icosahedral environment, are very similar and exhibit a broad pseudo-gap near E_F. In contrast, the local DOS at Mn(1), Mn(3) and Mn(4) exhibit no pseudo-gap. Note that the local DOS at Mn(3) and (4) are nearly identical, as expected from their similar structural environment (one Mn and eleven Al first neighbours; see table 1). The different local DOS at Mn(1) might result from the lower coordination of that site (nine Al). The spin-polarized self-consistent calculation leads to a non-magnetic state ($S = 0$) at the five Mn sites. Note that the convergence of the moment to zero at sites Mn(3) and Mn(4) is very slow, which might indicate that these atoms are close to a magnetic non-magnetic transition and that the energy differences between the magnetic and non-magnetic configurations are small.

5. Discussion

Let us briefly recall the present state of knowledge on the origin of magnetism in AlMn and AlPdMn quasicrystals and related phases which are characterized by a strong sp–d hybridization [8–10, 36, 38].

The magnetic state of a transition atom in a metallic host results from the competition between the Coulomb interaction, favouring a magnetic state, and the kinetic energy of the d electrons, increased by sp–d hybridization and minimized in a non-magnetic state. For small concentration of transition atoms, this situation is described by the standard virtual-bound-state (VBS) picture. The case of a Mn atom embedded in a fcc Al matrix has been widely debated [39]: most of the authors conclude that it is a magnetic state, in qualitative agreement with experimental results on dilute AlMn alloys [40]. Besides, it has been shown that the local lattice relaxation around a Mn impurity strongly affects the moment value [41]. Recent calculations [9] show that the VBS picture holds even at relatively large Mn concentration and that all the Mn atoms carry a magnetic moment ($\sim 2.5\ \mu_B$) in a fcc $Al_{0.86}Mn_{0.14}$ solid solution.

In quasicrystals and approximants, the standard virtual-bound-state picture has to be modified in order to account for the presence of a pseudo-gap in the density of states around the Fermi level [8]. The splitting of sp states into bonding and antibonding states, due to the diffraction by Bragg planes, influences the moment formation and the criterion for moment stability must then be modified [42]. The main result is that, in the presence of a pseudo-gap in their local DOS, Mn atoms are expected to be stable in a non-magnetic state. In the absence of a pseudo-gap, the moment formation can still be described by the standard virtual-bound-state model, and Mn atoms are then susceptible to carrying a moment, like in fcc Al. The formation of magnetic moments on Mn atoms is therefore extremely sensitive to their local environment. The same conclusion is drawn from self-consistent local spin-density calculations performed by Hafner *et al* on models of icosahedral and decagonal AlMn phases [9, 10]. By examining the local DOS at all Mn sites, these authors found that the formation of a magnetic moment is governed by a local Stoner criterion, satisfied only at certain sites. (Strictly speaking such a criterion is non-exact, because of the pronounced non-rigid behaviour of the bands in the presence of a magnetic moment [42].) The presence of Mn–Mn first neighbours has thus been found to favour the moment formation [9]. In addition, medium-range Mn–Mn distances also play a role [42]. Provided that the Mn concentration is not too small, the pseudopotential which scatters the valence electrons is mainly due to the Mn atoms themselves (the Al pseudopotential being much weaker) and the pseudo-gap results mainly from the diffraction of the valence electrons by the Mn atoms. This effect can be analysed in terms of a long-range effective pair potential (up to ~ 10 Å) [42, 43] which moreover depends on the magnetic state of Mn atoms. Therefore, the pseudo-gap in the local DOS at Mn atoms, and in consequence their magnetic

state, also depend on the medium-range order of the Mn atoms [42].

Let us now examine the origin of magnetism in the 1/1 approximant. From the arguments recalled above, the non-magnetic character of Mn(4) atoms, found in spin-polarized LMTO calculations, directly results from the pseudo-gap observed in their local DOS, calculated without spin polarization. In contrast, the presence of a moment on Mn(5) atoms is made possible by the absence of pseudo-gap in their local DOS leading to a relatively high $N(E_F)$. The theoretical spin value of Mn(5), $S \sim 0.35$ (with $g = 2$), is in reasonable agreement with the measured one: from the Curie constant in the temperature range [30 K–300 K] (table 2), one obtains then $S = 0.56$, using $g = 2$ and $c^\star = 0.093$ ($c^\star/c = 2/3$). Only a qualitative comparison of these two values is meaningful. The local density approximation, on which are based LMTO calculations, leads to an underestimate of the magnetic moment when the sp–d hybridization is strong. In addition, all moments were assumed to be parallel at $T = 0$ in the LMTO calculation. This is probably not the case: the saturation magnetization deduced from the spin value measured above T_c ($M_{sat} = c^\star N_a g \mu_B S/M_a = 14.7$ emu g^{-1}) is larger than the magnetization measured at 5 K in 50 kOe (4.4 emu g^{-1}). The saturation is therefore far from being reached in these experimental conditions, as is indeed confirmed by the shape of the magnetization curve which shows no tendency to saturation. This behaviour, as well as the difference observed between Θ and T_c (section 3.3), suggests the existence of antiferromagnetic interactions competing with the dominant ferromagnetic ones which might result in a non-collinear state below T_c. The ferromagnetism observed in the 1/1 approximant is probably a specific feature of this phase. A site similar to Mn(5), i.e. forming a small-edge icosahedron, is not found in other approximant phases and is not an ingredient of QC models [44]. The moment formation on such a site is certainly influenced by the presence of five Mn first neighbours. Nevertheless it should be noted that ferromagnetic quasicrystalline phases have been found in the Al–Pd–Mn–B system when a few per cent of Al (between 3 and 6 at.%) are substituted for with B [45]. These metastable quaternary alloys are characterized by a high Curie temperature ($\sim$500 K) and a saturation magnetization of $\sim 1\ \mu_B$ per Mn atom, assuming that all the Mn atoms carry the same moment. Besides, NMR studies [46] have shown that non-magnetic Mn atoms coexist with the magnetic ones. However, these striking properties, compared to the spin-glass state observed at $\sim$10 K in the corresponding AlPdMn QC phase, remain difficult to interpret in the absence of a structural model.

In the T-$Al_{79.5}Pd_{5.1}Mn_{15.4}$ phase, the five Mn sites are found to be non-magnetic in the spin-polarized self-consistent calculation. Note that the non-magnetic character of Mn(2) and Mn(5) is a direct consequence of the pseudo-gap in their local DOS and could have been predicted *a priori*. In contrast, no pseudo-gap is observed in the local DOS at Mn(1), Mn(3) and Mn(4) and the spin-polarized calculations are required to establish that these sites are non-magnetic. The composition of the LMTO model is very close to that of the Mn-poor T-$Al_{78.5}Pd_{4.9}Mn_{16.6}$ sample. The absence of magnetic moments in this sample is then in full agreement with the theoretical calculation. When going from this Mn-poor sample to the Mn-rich T-$Al_{73.1}Pd_{5.2}Mn_{21.7}$ phase, the composition changes lead to the partial occupancy of sites TM(1) to TM(5) by Mn atoms (see table 1 and figure 1). Schematically, one can consider two hypotheses. Either some of the Mn sites, already occupied in the Mn-poor sample, become magnetic when Mn atoms are added at sites TM(1) to TM(5), or moments are present on some of the Mn atoms occupying these TM sites. Unfortunately, no LMTO calculation of this Mn-rich T phase can be performed because of the chemical disorder and only qualitative arguments can be given. We can exclude the case where all the Mn atoms occupying one of the Wyckoff positions Mn(1) to Mn(5) would be magnetic. This hypothesis would lead to an ordered magnetic state and is incompatible with the observation of a spin-glass transition. However, because of the chemical disorder, the environment of the Mn atoms

occupying a given Mn site is not constant in the Mn-rich T phase and the existence of moments on a fraction of them cannot be excluded. On the other hand, if Mn atoms at sites TM(1) to TM(5) are magnetic, the chemical disorder resulting from the partial occupation of these sites by Al and Mn atoms leads to a disordered repartition of the magnetic Mn atoms. The local environments of these TM sites (table 1) are similar and no strong differences are observed which would allow one to particularize one of them. In contrast, systematic differences are found between the environments of Mn atoms at TM sites and at pure Mn sites. The former ones are characterized by larger Al–Mn distances, as well as the presence of a small fraction of Pd first neighbours (except for TM(5)) and a larger averaged number of Mn–Mn pairs. According to the general arguments recalled above, increasing the Mn–Al distance induces a decrease of the sp–d hybridization which favours magnetism. Besides, both Mn–Mn [9] and Mn–Pd [10] pairs were found to favour magnetism in models of QC phases. It seems then reasonable to conclude that the magnetism of the Mn-rich T phase is due to the Mn atoms at the TM sites. Then $c^{\star}/c = 0.29$ and one obtains $S \sim 1$ from the measured Curie constant in the range [30 K–100 K], assuming that all the magnetic Mn atoms carry the same spin.

The spin-polarized band-structure calculations of the T-$Al_{79.5}Pd_{5.1}Mn_{15.4}$ phase can be compared with those performed on the binary T-Al_3Mn phase [9, 37]. The five Mn sites of the ternary phase are also occupied by Mn atoms in the binary phase [29]: Mn(1) to Mn(4) have the same labels but Mn(5) in the ternary phase corresponds to Mn(7) in the binary phase. There are sites occupied by an Al/Mn mixture in the binary T phase [29] but they were assumed to be only occupied by Al atoms in the calculation of reference [9]. Then the only difference between the two calculated structures is the existence of two additional Mn sites in the binary T phase located in the $y = 1/4$ plane (labelled Mn(5) and Mn(6) in reference [29]). The Mn(2), Mn(3), Mn(4), Mn(5) and Mn(6) atoms form a small pentagon and are each surrounded by ten Al and two Mn atoms forming an icosahedral shell. Spin-polarized calculations lead to a substantial moment on Mn(5) and Mn(6) atoms [9] (0.66 and 1 μ_B respectively) and not on the other Mn atoms, with the possible exception of Mn(2). These results are not in contradiction with the non-magnetic character of the T-$Al_{79.5}Pd_{5.1}Mn_{15.4}$ phase, because the two magnetic Mn sites in the T-Al_3Mn phase are occupied by Al in the ternary phase. However, the predicted Curie term is not observed in susceptibility measurements on the T-Al_3Mn phase [47].

6. Conclusions

In most AlMn and AlPdMn crystalline phases, the Mn atoms have been found to be non-magnetic. This is the case for the $Al_{12}Mn$, Al_6Mn, λ-$Al_{4.5}Mn$, α-$Al_{72.45}Mn_{17.4}Si_{10.15}$ and β-$Al_{73}Mn_{21}Si_6$ phases [15], as well as the ξ' and 2/1 AlPdMn phases studied here. Magnetic phases, such as the 1/1-$Al_{68}Pd_{11}Mn_{14}Si_7$ cubic approximant and the Mn-rich T-$Al_{73.1}Pd_{5.2}Mn_{21.7}$ phase studied here, or the μ-Al_4Mn phase [15] are exceptions. In all these phases, we have shown that only particular Mn sites carry a magnetic moment and that they coexist with non-magnetic ones. In quasicrystalline phases also, only a small fraction of the Mn atoms carry moments. One must then wonder to what extent the study of these magnetic approximants sheds light on the magnetism of QC.

Indeed, the magnetic behaviour of the Mn-rich T phase is very similar to that of decagonal and icosahedral phases in the Al–Mn and Al–Pd–Mn systems [4, 5, 7]. It is striking to observe that, for a given concentration of magnetic Mn, similar spin-glass temperatures are observed in all these phases [7]. Despite strong variations of the total DOS at the Fermi level among all these phases, the amplitude of the RKKY coupling is therefore nearly constant, and close to the value measured for CuMn spin glasses [7]. (For example, the spin-glass temperature of a CuMn alloy with the same Curie constant as the Mn-rich T phase is equal to 12.5 K.) This

surprising result can be explained by the fact that the local DOS at the magnetic sites has to be considered in the computation of the RKKY coupling [48]. It confirms therefore that magnetic Mn are characterized by a similar and relatively high local DOS at the Fermi level in all these phases. Because of the similarity between the structure of the T and decagonal phases [29, 37], we are led to assume that the decagonal phase contains Mn atoms with an environment similar to that of TM sites in the T phase which favours magnetism. As noted previously, it is difficult to separate the effects of a relatively loose Mn–Al coordination and those of d–d couplings between Mn first neighbours. Note that the magnetic site identified in the μ-Al_4Mn phase has a different nature. It is characterized by a very low coordination (seven Al atoms). The presence of a moment on this site is made possible by the low sp–d hybridization associated with this low coordination, but as shown in references [15, 42] the relative positions of Mn atoms must also play a role. In addition, one should emphasize that Mn atoms surrounded by twelve Al atoms, or eleven Al atoms and one Mn atom, in an icosahedral environment, are found to be non-magnetic in the T phase as well as in the μ phase. This behaviour must be linked with the strong sp–d hybridization associated with the compact environment of these Mn atoms. In conclusion, the comparison with approximant phases shows that only a few specific Mn sites are likely to be responsible for the observed magnetism in quasicrystalline phases.

References

[1] Matsuo S, Nakano H, Ishimasa T and Fukano Y 1989 *J. Phys.: Condens. Matter* **1** 6893
[2] Lin C R, Lin S T, Wang C R, Chou S L, Horng H E, Cheng J M, Yao Y D and Lai S C 1997 *J. Phys.: Condens. Matter* **9** 1509
[3] Lanco P, Klein T, Berger C, Cyrot-Lackmann F, Fourcandot G and Sulpice A 1992 *Europhys. Lett.* **18** 227
[4] Saito K, Matsuo S, Nakano H, Ishimasa T and Mori M 1994 *J. Phys. Soc. Japan* **63** 1940
Kobayashi A, Matsuo S, Ishimasa T and Nakano H 1997 *J. Phys.: Condens. Matter* **9** 3205
[5] Satoh M, Hattori Y, Kataoka N, Fukamichi K and Goto T 1994 *Mater. Sci. Eng.* A **181+182** 801
[6] Chernikov M A, Bernasconi A, Beeli C, Schilling A and Ott H R 1993 *Phys. Rev.* B **48** 3058
Lasjaunias J C, Sulpice A, Keller N, Préjean J J and de Boissieu M 1995 *Phys. Rev.* B **52** 886
[7] Préjean J J, Lasjaunias J C, Sulpice A, Mayou D and Berger C 1995 *Proc. 5th Int. Conf. on Quasicrystals* ed C Janot and R Mosseri (Singapore: World Scientific) p 510
[8] Trambly de Laissardière G, Mayou D and Nguyen Manh D 1993 *Europhys. Lett.* **21** 25
Trambly de Laissardière G, Nguyen Manh D, Magaud L, Julien J P, Cyrot-Lackmann F and Mayou D 1995 *Phys. Rev.* B **52** 7920
[9] Hafner J and Krajči M 1998 *Phys. Rev.* B **57** 2849
[10] Krajči M and Hafner J 1998 *Phys. Rev.* B **58** 14 110
[11] Bratkovsky A M, Smirnov A V, Nguyen Manh D and Pasturel A 1995 *Phys. Rev.* B **52** 3056
[12] Elser V and Henley C 1985 *Phys. Rev. Lett.* **55** 2883
Guyot P and Audier M 1985 *Phil. Mag.* B **52** L15
Henley C and Elser V 1986 *Phil. Mag.* B **53** L59
[13] Mackay A L 1962 *Acta Crystallogr.* **15** 916
Bergman G, Waugh J L T and Pauling L 1957 *Acta Crystallogr.* **10** 254
[14] Mayou D, Berger C, Cyrot-Lackmann F, Klein T and Lanco P 1993 *Phys. Rev. Lett.* **70** 3915
[15] Simonet V, Hippert F, Audier M and Trambly de Laissardière G 1998 *Phys. Rev.* B **58** 8865
[16] Sugiyama K, Kaji N and Hiraga K 1998 *Z. Kristallogr.* **213** 168
[17] Sugiyama K, Kaji N and Hiraga K 1998 *Z. Kristallogr.* **213** 90
[18] Boudard M, Klein H, de Boissieu M, Audier M and Vincent H 1996 *Phil. Mag.* A **74** 939
[19] Klein H, Boudard M, de Boissieu M, Audier M, Vincent H, Beraha L and Duneau M 1996 *Phil. Mag. Lett.* **75** 197
[20] Matsuo Y, Kaneko M, Yamanoi T, Kaji N, Sugiyama K and Hiraga K 1997 *Phil. Mag. Lett.* **76** 357
[21] Yokoyama Y, Tsai A P, Inoue A and Masumoto T 1991 *Mater. Trans. JIM* **22** 1089
[22] Audier M, Durand-Charre M and de Boissieu M 1993 *Phil. Mag.* B **68** 607
[23] Gödecke T and Lück R 1995 *Z. Metallk.* **86** 1095
[24] Klein H, Durand-Charre M and Audier M 1999 *J. Alloys Compounds* at press

[25] Klein H, Audier M, Boudard M, de Boissieu M, Beraha L and Duneau M 1996 *Phil. Mag.* A **73** 309
Beraha L, Duneau M, Klein H and Audier M 1997 *Phil. Mag.* A **76** 587
[26] Waseda A, Morioka H, Kimura K and Ino H 1992 *Phil. Mag. Lett.* **65** 25
[27] Cooper M and Robinson K 1966 *Acta Crystallogr.* **20** 614
[28] Samson S 1968 *Structural Chemistry and Molecular Biology* ed A Rich and N Davidson (San Fransisco, CA: Freeman) p 687
Shoemaker D P and Brink-Shoemaker C 1988 *Aperiodic Crystals* vol 1, ed M V Jaric (Boston, MA: Academic) p 1
Kreiner G and Franzen H F 1997 *J. Alloys Compounds* **261** 83
Audier M, Durand-Charre M, Laclau E and Klein H 1995 *J. Alloys Compounds* **220** 225
Schenk T, Durand-Charre M and Audier M 1998 *J. Alloys Compounds* **281** 249
[29] Hiraga K, Kaneko M, Matsuo Y and Hashimoto S 1993 *Phil. Mag.* B **67** 193
[30] Cyrot-Lackmann F 1997 *Solid State Commun.* **103** 123
[31] Simonet V, Hippert F, Klein H, Audier M, Bellissent R, Fisher H, Murani A P and Boursier D 1998 *Phys. Rev.* B **58** 6273
[32] Fisher K H and Hertz J A 1991 *Spin Glasses* (Cambridge: Cambridge University Press)
[33] Andersen O K 1975 *Phys. Rev.* B **12** 3060
Skriver H L 1984 *The LMTO Method* (New York: Springer)
[34] von Barth U and Hedin L 1972 *J. Phys. C:Solid State Phys.* **5** 1629
[35] Krajči M, Windisch, Hafner J, Kresse G and Mihalkovič M 1995 *Phys. Rev.* B **51** 17 355
[36] Fujiwara T and Yokokawa T 1991 *Phys. Rev. Lett.* **66** 333
Fujiwara T, Yamamoto S and Trambly de Laissardière G 1993 *Phys. Rev. Lett.* **71** 4166
Trambly de Laissardière G and Fujiwara T 1994 *Phys. Rev.* B **50** 5999
[37] Krajči M, Hafner J and Mihalkovič M 1997 *Phys. Rev.* B **55** 843
[38] Belin E, Dankhazi Z, Sadoc A and Dubois J M 1994 *J. Phys.: Condens. Matter* **6** 8771
[39] Deutz J, Dederichs P H and Zeller R 1981 *J. Phys. F: Met. Phys.* **11** 1787
Bagayoko D, Brener N, Kanhere D and Callaway J 1987 *Phys. Rev.* B **36** 9263
Yang Jinlong, L Huibin, Wang Kelin, Donà dalle Rose L F and Toigo F 1991 *Phys. Rev.* B **44**, 10 508
Liu F, Khanna S N, Magaud L, Jena P, de Coulon V, Reuse F, Jaswal S S, He X G and Cyrot-Lackmann F 1993 *Phys. Rev.* B **48** 1295
[40] Cooper J R and Miljak M 1976 *J. Phys. F: Met. Phys.* **6**, 2151
[41] Guenzburger D and Ellis D E 1994 *Phys. Rev.* B **49** 6004
[42] Trambly de Laissardière G and Mayou D 1999 *Introduction to the Physics of Quasicrystals* ed J B Suck (Berlin: Springer) at press
Trambly de Laissardière G and Mayou D 1999 *Proc. 7th Int. Conf. on Quasicrystals; Physica* B at press
[43] Zou J and Carlsson A E 1993 *Phys. Rev. Lett.* **70** 3748
[44] Boudard M, de Boissieu M, Janot C, Heger G, Beeli C, Nissen H U, Vincent P, Ibberson R, Audier M and Dubois J M 1992 *J. Phys.: Condens. Matter* **4** 10 149
[45] Yokoyama Y, Inoue A and Masumoto T 1994 *Mater. Sci. Eng.* A **181+182** 734
[46] Shinohara T, Yokoyama Y, Sato M, Inoue A and Masumoto T 1993 *J. Phys.: Condens. Matter* **5** 3673
[47] Volkov P and Poon S J 1995 *Phys. Rev.* B **52** 12 685
[48] Roche S and Mayou D 1995 *Proc. 5th Int. Conf. on Quasicrystals* ed C Janot and R Mosseri (Singapore: World Scientific) p 493
Roche S and Mayou D 1999 *Phys. Rev.* B **60** 322